PAPER

Check for updates

Highly active nanoparticle enhanced rapid adsorption-killing mechanism to combat multidrug-resistant bacteria†

Yunyun Xue,‡[ad] Zihao Zhao,‡[ad] Wenbo Huang,‡[b] Zelin Qiu,[a] Xiao Li,[b] Yu Zhao,[a] Chuyao Wang,[a] Ronglu Cui,[a] Shuyang Shen,[a] Hua Tian,[a] Lifeng Fang, [ID] *[a] Rong Zhou*[bc] and Baoku Zhu [ID] *[ad]

Contact-killing surfaces with the ability to rapidly adsorb and kill microorganisms are desperately needed since the rapid outbreak of multidrug-resistant (MDR) bacteria poses a serious threat to human health. Therefore, a series of amphiphilic nanoengineered polyquaterniums (ANPQs) were synthesized, and immobilizing ANPQs onto equipment surfaces provided a simple method for preventing microbial infections. The strong charge-positive property of ANPQ offered the possibility of rapid adsorption and efficient killing, such that all bacteria are adsorbed after 10 seconds of contact with ANPQ-treated fabrics, and more than 99.99% of pathogens are killed within 30 seconds. Surprisingly, the adsorption-killing mechanism made it difficult for bacteria to develop resistance to ANPQ coating, even after long-term repeated treatment. Importantly, in a Methicillin-resistant *Staphylococcus aureus* infection model, ANPQ-treated fabrics exhibited a potent anti-infectious performance while remaining nontoxic. It is envisaged that the strategy of using ANPQ coating undoubtedly provides a promising candidate for fighting MDR strains.

1 Introduction

Owing to the prolonged abuse of antibiotics, the pandemic of antimicrobial resistance has been greatly concerning.[1,2] Notably, hospital-acquired infections caused by multidrug-resistant (MDR) strains have endangered patient safety, protracted hospitalization periods, escalated treatment expenses, and resulted in elevated rates of mortality and morbidity.[3,4] Contamination of medical implants and equipment surfaces with MDR pathogens has emerged as a severe issue in the healthcare sector.[3,4] Urgent measures are imperative to devise tactics that can realize surfaces with rapid adsorption and killing mechanisms.

[a] *Department of Polymer Science and Engineering, ERC of Membrane and Water Treatment (MOE), Key Laboratory of Macromolecular Synthesis and Functionalization (MOE), Zhejiang University, Hangzhou, 310027, China. E-mail: fanglf@zju.edu.cn*
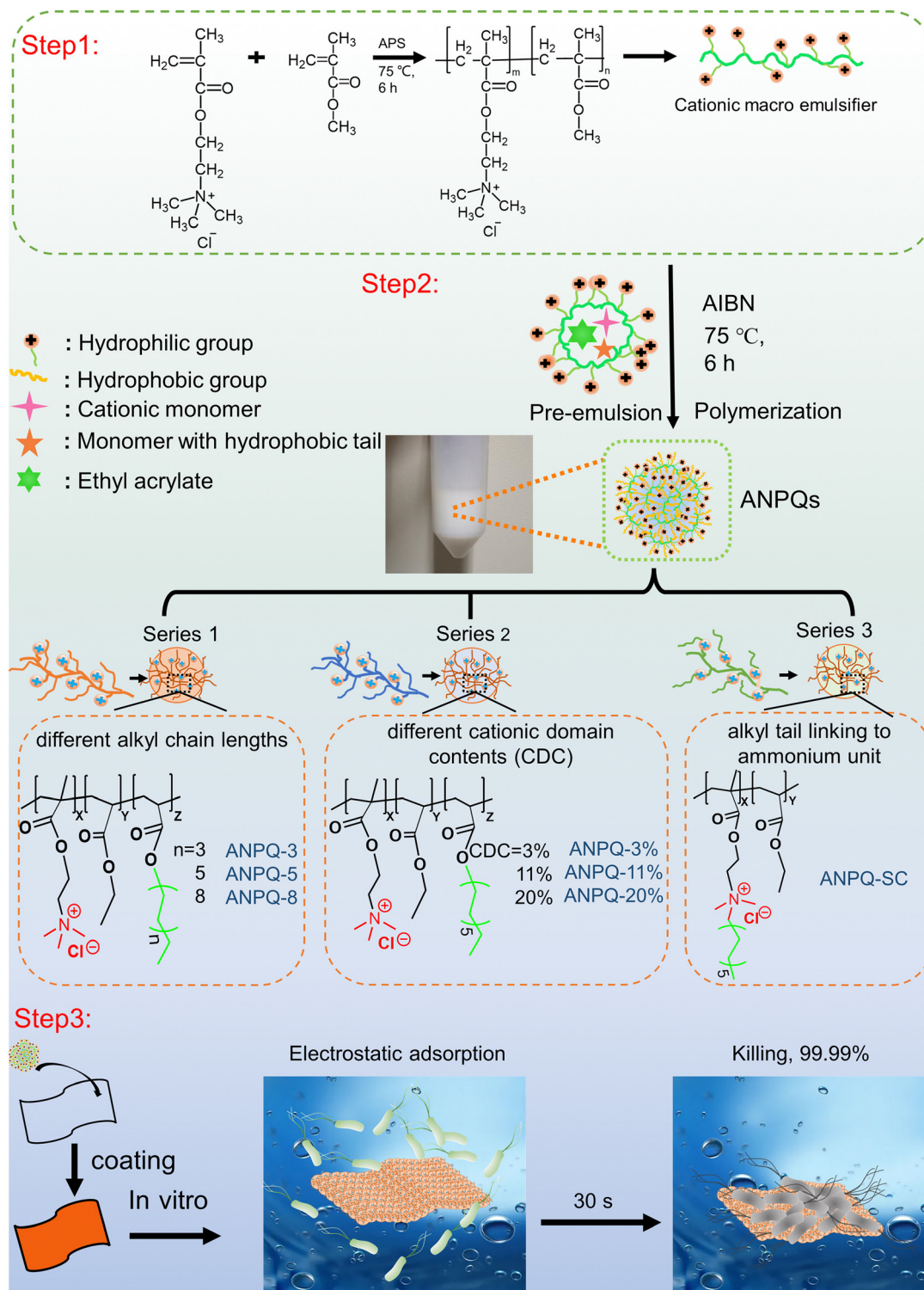
[b] *State Key Laboratory of Respiratory Disease, National Clinical Research Center for Respiratory Disease, Guangzhou Institute of Respiratory Health, the First Affiliated Hospital of Guangzhou Medical University, Guangzhou Medical University, Guangzhou 510182, China. E-mail: zhourong@vip.163.com*

[c] *Guangzhou Laboratory, Guangzhou 510182, China*

[d] *Center of Healthcare Materials, Shaoxing Institute, Zhejiang University, Shaoxing, 312000, China. E-mail: zhubk@zju.edu.cn*

† Electronic supplementary information (ESI) available. See DOI: https://doi.org/10.1039/d3tb01105d

‡ Equally contributing first authors.

To tackle the aforementioned challenge, endeavors have been undertaken to design diverse strategies, such as coating materials with antimicrobial agents, such as zinc oxide nanoparticles, copper nanoparticles, and silver nanoparticles.[5–8] Despite the promising antibacterial efficacy, the leakage of metal ions from metallic nanoparticles may pose a threat to the environment and cause excessive buildup in tissues, which could potentially endanger human health.[9,10]

An alternative option is to employ bactericidal contact-killing surfaces, which execute bacterial death through various mechanisms upon adhesion. Among the most prevalent selections for developing such surfaces are antimicrobial peptides, quaternary ammonium compounds, and polycations.[11–14] Benefitting from the advantages of cost-effectiveness, ease of scale-up, and less susceptibility to antibiotic resistance, cationic polymer nanoparticles have recently gained widespread attention.[15–20] In contrast to monovalent systems, these nanoparticles have multiple ligands that can bind to several receptors on microbial membranes, leading to stronger interactions.[19,21] The higher local cationic charge and hydrophobic bulk in the assembled form enable these nanoparticles to establish improved electrostatic contact with the microbial membrane and confer enhanced antibacterial activity.[19,21] However, the majority of synthetic polymer nanoparticles documented in the literature are water-soluble,[22] which can lead to

Scheme 1 Synthesis of ANPQs and antibacterial mechanism of ANPQ-treated fabrics.

uneven release kinetics, reservoir exhaustion concerns, and environmental issues.[23–25] Therefore, it is critical to create water-insoluble polymer nanoparticles for bactericidal contact-killing surfaces.

In this study, a series of amphiphilic nanoengineered polyquaterniums (ANPQ) containing cationic groups and hydrophobic alkyl tails were designed (Scheme 1). *Escherichia coli* (*E. coli*), *Staphylococcus aureus* (*S. aureus*), *Pseudomonas aeruginosa* (PAO1), and Methicillin-resistant *Staphylococcus aureus* (MRSA), which are the most common causes of hospital-acquired infections, were used to evaluate *in vitro* antimicrobial activities of ANPQ. The antibacterial activity of ANPQs was

This journal is © The Royal Society of Chemistry 2023

J. Mater. Chem. B, 2023, **11**, 7750–7765 | **7751**

primarily derived from electrostatic adsorption and hydrophobic interaction, severely resulting in membrane translocation and membrane damage. The ability of ANPQ-treated fabrics to promote rapid adsorption and high-efficiency pathogen killing was evaluated. In the presence of a 1/4-fold MBA concentration of ANPQ-11%, *E. coli* ATCC 8099, *S. aureus* ATCC 6538, PAO1, and MRSA cells were passed, and MBA was measured at each passage. Importantly, ANPQ-treated fabrics demonstrated fast and high-effective antibacterial activity against MDR bacteria *in vitro* and MRSA infection *in vivo*, with negligible toxicity and drug resistance, indicating a high potential for biomedical applications.

2 Experimental section

2.1 Synthesis of amphiphilic nanoengineered polyquaterniums (ANPQs)

In conventional micro-emulsion polymerization, the addition of a significant amount of small molecule emulsifiers necessitated a complex post-processing procedure. Therefore, in this work, ANPQs were synthesized by self-emulsifying polymerization of macromolecular emulsifiers, which eliminated the complex post-processing of small molecule emulsifiers.

Synthesis of a cationic macro emulsifier (CME). As shown in Scheme 1 (step 1), briefly, 5.00 g methyl methacrylate (MMA), 2.86 g methacrylatoethyl trimethyl ammonium chloridecan (MTAC), 0.10 g ammonium persulfate (APS), and appropriate amount of ultrapure water were added into a three-necked flask with dropping funnels, reflux condenser, and mechanical stirrer (GZ120-S, Shanghai). Then, the mixture was reacted at 75 °C for 6 h under continuous mechanical stirring (300 rpm) and an N$_2$ atmosphere. As shown in Fig. S2 (ESI†), the CME was synthesized successfully.

Synthesis of antibacterial monomers. In short, 2-(dimethylamino)ethyl methacrylate and iodododecane were dissolved in ethanol at a molar ratio of 1:1.5, and the reaction was carried out at 60 °C for 24 hours under magnetic stirring (300 rpm). Finally, the product was precipitated and washed three times with ice ether, followed by vacuum drying to obtain the intermediate monomer (Q-SC).

Synthesis of ANPQs. For comparison, 7 kinds of different antibacterial polymer emulsions (ANPQ-8, ANPQ-12, ANPQ-18,

ANPQ-3%, ANPQ-11%, ANPQ-20%, ANPQ-SC) were prepared by adjusting antibacterial monomers (*n*-octyl acrylate (C8), dodecyl acrylate (C12), and octadecyl acrylate (C18)), contents of MTAC (3 mol%, 11 mol%, and 20 mol%), and contents of Q-SC (43 mol%). The recipe is given in Table 1. As illustrated in Scheme 1 (step 2), for instance, 63 mol% ethyl acrylate, 11 mol% MTAC, and 26 mol% C8 were pre-emulsified in a three-necked flask using an appropriate amount of ultrapure water and 2 wt% CME (based on the total acrylic monomers) as an emulsifier. Then, after adding 1 wt% AIBN (based on the total acrylic monomers), the polymerization was carried out at 75 °C for 6 h under mechanical stirring (300 rpm) and an N$_2$ atmosphere. ANPQ emulsion was purified by dialysis with PBS before use.

Monomer conversion was measured by the weighing method. Briefly, a certain amount of ANPQ emulsions was demulsified using ethanol and cleaned with water and acetone repeatedly to remove unreacted monomers and impurities. The obtained polymer was dried in a vacuum drying oven at 80 °C to constant weight. The monomer conversion (%) was calculated using the formula: $M_C = (W_0 - W_1)/W_0 \times 100\%$. W_0 and W_1 are the weights of ANPQ emulsions before and after treatment, respectively.

2.2 Fabrication of antibacterial coatings

In brief, ANPQ emulsion was diluted to 1 wt% using ultrapure water at room temperature. Polypropylene (PP) nonwoven fabrics were then immersed in the emulsion for 30 minutes. Then, the treated fabrics were taken out and dried under 150 °C for 10 min. Afterward, the ANPQ-treated fabrics were ultrasonically cleaned (37 °C, 5 min) to remove the superficially unstable nanoparticles, and finally dried under 150 °C for 10 min. By referring to the previous method,[26] the coating amount of ANPQs was calculated according to eqn (1):

$$\text{Coating amount (g m}^{-2}) = (M_1 - M_0)/S \qquad (1)$$

where M_0 and M_1 are the weights of the PP-nonwoven fabrics before and after treatment, respectively; *S*: is the specific surface area of the fabric. The PP-nonwoven fabrics coated with ANPQs were termed as PP$_{ANPQs}$. Each reported value was represented by the means of five samples.

Table 1 A summary of the experimental description for ANPQs

Antibacterial polymers		Alkyl chain component	Cationic domain component	EA (mol%)	ASC (%)	MC (%)
ANPQ-6	Different alkyl chain lengths	26 mol% C8	11 mol%	63	31	98.6
ANPQ-10		26 mol% C12	11 mol%	63	28	98.8
ANPQ-16		26 mol% C18	11 mol%	63	27	87.5
ANPQ-3%	Different cationic domain	29 mol% C12	3 mol%	68	28	99.5
ANPQ-11%		26 mol% C12	11 mol%	63	28	98.8
ANPQ-20%		23 mol% C12	20 mol%	57	26	97.8
ANPQ-SC	Alkyl tail linking to ammonium unit	43 mol% Q-SC	43 mol% Q-SC	57	29	82.5

Note: ASC represents actual solid content. MC represents monomer conversion (%).

7752 | *J. Mater. Chem. B*, 2023, **11**, 7750–7765

This journal is © The Royal Society of Chemistry 2023

2.3 Antibacterial assays of ANPQs

2.3.1 Bacterial cultures. As the typical etiological bacteria, Gram-negative bacteria (*E. coli* ATCC 8099, PAO1) and Gram-positive bacteria (*S. aureus* ATCC 6538, MRSA) supplied by the Chinese Academy of Inspection and Quarantine (Beijing, China) were applied for the antibacterial assay. A single colony of fourth-generation bacteria was transferred to a 250 mL Erlenmeyer flask with 20 mL LB medium and incubated in a shaking incubator at 37 °C and 200 rpm overnight.

2.3.2 Minimum bactericidal concentration (MBC) test. The overnight culture of bacteria was diluted to the target concentration ($\sim 10^6$ CFU mL^{-1}) using the LB liquid medium for use. ANPQ emulsions were added to polypropylene tubes and diluted with LB medium to the desired concentration. Negative controls of the comprising cells were without the treatment. Positive controls only comprised LB culture without cells. After incubation at 37 °C for 22–24 h, the minimum bactericidal concentration (MBC) was taken as the lowest ANPQ concentration required to eliminate at least 99.99% of viable bacteria ($\sim 10^6$ CFU mL^{-1}). At least three biologically independent replicates were performed per sample using two technical replicates.

2.3.3 Minimum bactericidal amount (MBA) test. After 2-fold serial dilution, 100 μL of ANPQs emulsion was added to the well of a 96-well plate and dried in a vacuum oven at 37 °C. To determine the minimum bactericidal amount (MBA; mg cm^{-2} present in the well), 200 μL bacteria ($\sim 10^6$ CFU mL^{-1}) was added to the ANPQs coated wells and incubated at 37 °C for 24 h. Negative control groups were the blank wells containing an equal volume of bacteria suspension. Positive control groups were the solvent-dried wells containing an equal volume of liquid LB. Afterward, 100 μL aliquots from wells that had nearly no bacterial growth were plated on the agar plates and then incubated at 37 °C for colony counting. Three bio-independent replicates were performed using two technical replicates each time.

2.3.4 Bacterial cell morphology characterization. The bacterial suspension ($\sim 10^6$ CFU mL^{-1}) was incubated with ANPQs (concentration at MBC) at 37 °C for 60 min and then collected by centrifugation (10 000 rpm for 5 min). The collected bacterial pellets were fixed with glutaraldehyde solution (2.5%) overnight at 4 °C for further Scanning Electron Microscopy (SEM) (FESEM, S-4800, Japan) and Transmission Electron Microscopy (TEM, Thermo Scientific Talos L120C) observations.

2.4 Hemolysis assays of ANPQs

Fresh pig blood (sodium heparin as an anticoagulant) was purchased from Beijing Bersee Science and Technology CO. LTD (Beijing, China) and was used to evaluate the toxicity of ANPQs on normal cells *in vitro*. Due to the fact that red blood cells (RBCs) are the most fragile cells, the biocompatibility of ANPQs can be directly reflected through hemolytic activity. Firstly, RBCs were collected by centrifugation (3000 rpm, 5 min) and washed until the supernatant was clear and transparent. RBCs were diluted to 2 wt% with sterile saline for use.

Equal volume RBCs suspension was incubated with ANPQs emulsions at 37 °C for 60 min to obtain HC50, while 200 μL of RBC suspension was cultured with ANPQs coating at the same condition to calculate HA50%. HC50 and HA50 are defined as the concentration and the coating amount that lyses 50% of the red blood cells and releases hemoglobin, respectively. The experiments were performed in triplicate with two repeats.

2.5 Antibacterial assays of ANPQ-fabrics

2.5.1 Antibacterial ratio test. The antibacterial activities of ANPQ-treated fabrics were evaluated by the shake flask test according to ASTM E2149.2013a and ISO 20645-2004. An appropriate amount of the bacterial suspension was diluted to obtain OD$_{660}$ values between 0.060 and 0.075 and then diluted 100-fold for use. The test nonwoven fabrics (cut into 1 cm × 1 cm, weight 0.75 ± 0.02 g), 70 mL PBS, and 5 mL bacteria suspension were added to a 250 mL Erlenmeyer flask and incubated at 37 °C and 200 rpm for 18 h. The resulting suspensions were serially diluted 10-fold and transferred to LB agar plates for colony counting. The antibacterial ratio (AR) was obtained as follows eqn (2):

$$\text{Antibacterial ratio (\%)} = (A_0 - A)/A \times 100 \qquad (2)$$

where A is the colonies on treated fabrics and A_0 is the colonies on control samples, respectively.

2.5.2 Rapid adhesion test. The antibacterial mechanism of the ANPQ coating for enhancing rapid adsorption-killing was evaluated by the shake flask test according to ASTM E2149.2013a and ISO 20645-2004. The bacterial suspension was pipetted and diluted to OD$_{660}$ values between 0.060–0.075. The test nonwoven fabrics were cut into square sheets in size of 1 cm × 1 cm. 0.75 ± 0.02 g samples were added into a 250 mL Erlenmeyer flask filled with 70 mL PBS. 5 mL of the bacteria suspension was then added and shaken quickly for 10 seconds, 30 seconds, or 60 seconds. After that, the solution (solution A) was poured out and 50 mL eluent solution (solution B) was added to each of the jars as soon as possible. Solution A and solution B were diluted to a certain volume by 10-fold dilution and then transferred on LB agar plates for colony counting.

2.6 Rapid adsorption-killing mechanism

2.6.1 Crystal violet staining. Overnight cultures of bacteria were collected and washed with PBS and then resuspended in crystal violet staining solution (1%) at 37 °C. After 30 min of staining, the bacteria were collected and washed with PBS, and then diluted with PBS to $\sim 10^7$ CFU mL^{-1} for use. As the method described in Section 2.3.5, the rapid adsorption process of ANPQ-treated fabrics was recorded using a digital camera.

2.6.2 Live/dead staining. Live/Dead staining was performed using the LIVE/DEAD BacLight Viability Kit (Thermo-Fisher Scientific): SYTO 9 green fluorescent ($\lambda_{ex}/\lambda_{em}$ at 498/530 nm) is a membrane-permeant and propidium iodide (PI) red fluorescent dyes ($\lambda_{ex}/\lambda_{em}$ at 550/655 nm) only crosses

This journal is © The Royal Society of Chemistry 2023

J. Mater. Chem. B, 2023, **11**, 7750–7765 | **7753**

Journal of Materials Chemistry B

Paper

damaged cell membranes. ANPQ-treated fabrics were incubated with bacterial suspension ($\sim 10^7$ CFU mL^{-1}) using the same method described in Section 2.3.4. Then, the fabric samples were gently washed with PBS and stained with PI/SYTO 9 mixture solution for 20 min in the dark for further fluorescence microscope imaging (Laica, SP5, Germany).

2.6.3 Membrane integrity studies. Briefly, following the method described in Section 2.3.4, supernatants of bacterial culture after treatment with the fabric samples were obtained by centrifugation (10 000 rpm, 5 min). Supernatants were measured for spectrophotometric absorbance readings at 260 nm (corresponding to nucleic acids) and 280 nm (corresponding to proteins)[27,28] using a UV-vis spectrophotometer (UV2600, Shimadzu, Japan).

2.7 Inhibition zone test

According to the standard GB/T 31713-2015, a zone of inhibition could be used to evaluate the leaching of ANPQ coating. Briefly, test fabric samples were cut into a square shape with a side length of 1.5 cm × 1.5 cm. The bacterial suspension ($\sim 10^7$ CFU mL^{-1}) was uniformly spread on the broth agar using a sterile cotton swab, and the samples were placed. Then, the plates were incubated at 36 °C for 24 hours. After incubation, the inhibition zone was imaged by a digital camera. The antibacterial performance was evaluated by the diameter of the inhibition zone with three bioindependent replicates and two technical replicates each time.

2.8 Long-term stability

The long-term stability of antibacterial coatings was examined by leaching tests in 0.9% NaCl (aq). After continuous treatment time (1, 3, 5, 7, 9, and 30 days) under 37 °C and a shaking rate of 200 rpm. Antibacterial ratio, surface zeta potential, ATR-FTIR spectra, and SEM of antibacterial coatings were analyzed, respectively.

2.9 Antibacterial resistance test

E. coli ATCC 8099, *S. aureus* ATCC 6538, PAO1, and MRSA cells were passaged in the presence of 1/4 MBA of ANPQ-11% coating, and MBA was measured at each passage of bacteria. These manipulations were repeated 40 times consecutively to assess the effect of ANPQ-11% on the antibiotic resistance of *E. coli* ATCC 8099, while 10 times consecutively for the antibiotic resistances of *S. aureus* ATCC 6538, PAO1, and MRSA. To further investigate the biological mechanism of bacterial response to ANPQ-11%, each group was subjected to transcription sequencing after 40 passages of incubation under 1/4-fold MBA$_0$.

2.10 *In vivo* antibacterial activity

All animal experiments were performed under the Principles of Laboratory Animal Care (NIH Publication No. 86-23, revised 1985) and the guidelines of the Animal Care and Use Committee of Zhejiang University. Female mice (ICR, ~ 20 g) were provided by the Zhejiang Academy of Medical Sciences. After anesthetization, the mice's backs were shaved and sterilized.

Then, a circular whole-skin wound (8 mm in diameter) was created and all wounds were infected with 50 μL of MRSA suspension ($\sim 10^8$ CFU mL^{-1}). After infection for 24 h, the purulent wounds were treated with medical gauze, PP, and PP$_{ANPQ-11\%}$, respectively. Medical gauze served as a control. Treatments were performed every two days and the wound area was recorded by a digital camera. The wound size was calculated using ImageJ-Pro Plus 6.0 software. The wound ratio (%) was calculated by eqn (3):

$$\text{Wound ratio (\%)} = (A_t/A_0) \times 100\% \tag{3}$$

where A_0: initial wound size before treatment; A_t: wound size during treatment.

To evaluate the *in vivo* antibacterial activity, wound exudates were collected using sterile swabs and amplified in liquid LB solution at 37 °C for 4 h and then spread on agar plates for bacterial colony counting. On the 10th day, wound site tissues were collected and stained with hematoxylin and eosin (H&E), Masson's trichrome, and myeloperoxidase (MPO) for evaluating the actual antibacterial activity and wound healing. IL-6 expression in wound tissue from infected wounds was characterized by an ELISA kit.

2.11 *In vitro* and *in vivo* biosafety assay

The *in vitro* cytotoxicity was evaluated by incubating PP$_{ANPQ-11\%}$ with RBCs or L929 cells. An *in vitro* irritation test and a guinea pig maximization test were also performed. The experimental details are supplied in the SI. To evaluate the *in vivo* biosafety of PP$_{ANPQ-11\%}$, on the 10th day, blood and major organs (including heart, liver, spleen, lungs, and kidneys) were collected and stained with H&E.

Statistical analysis. All experiments were repeated at least three times and data were presented as mean ± standard deviation (SD). Statistical significance: $*p < 0.05$, $**p < 0.01$, $***p < 0.001$, NS: not significant, univariate analysis using Microsoft Excel statistical software.

3 Results and discussion
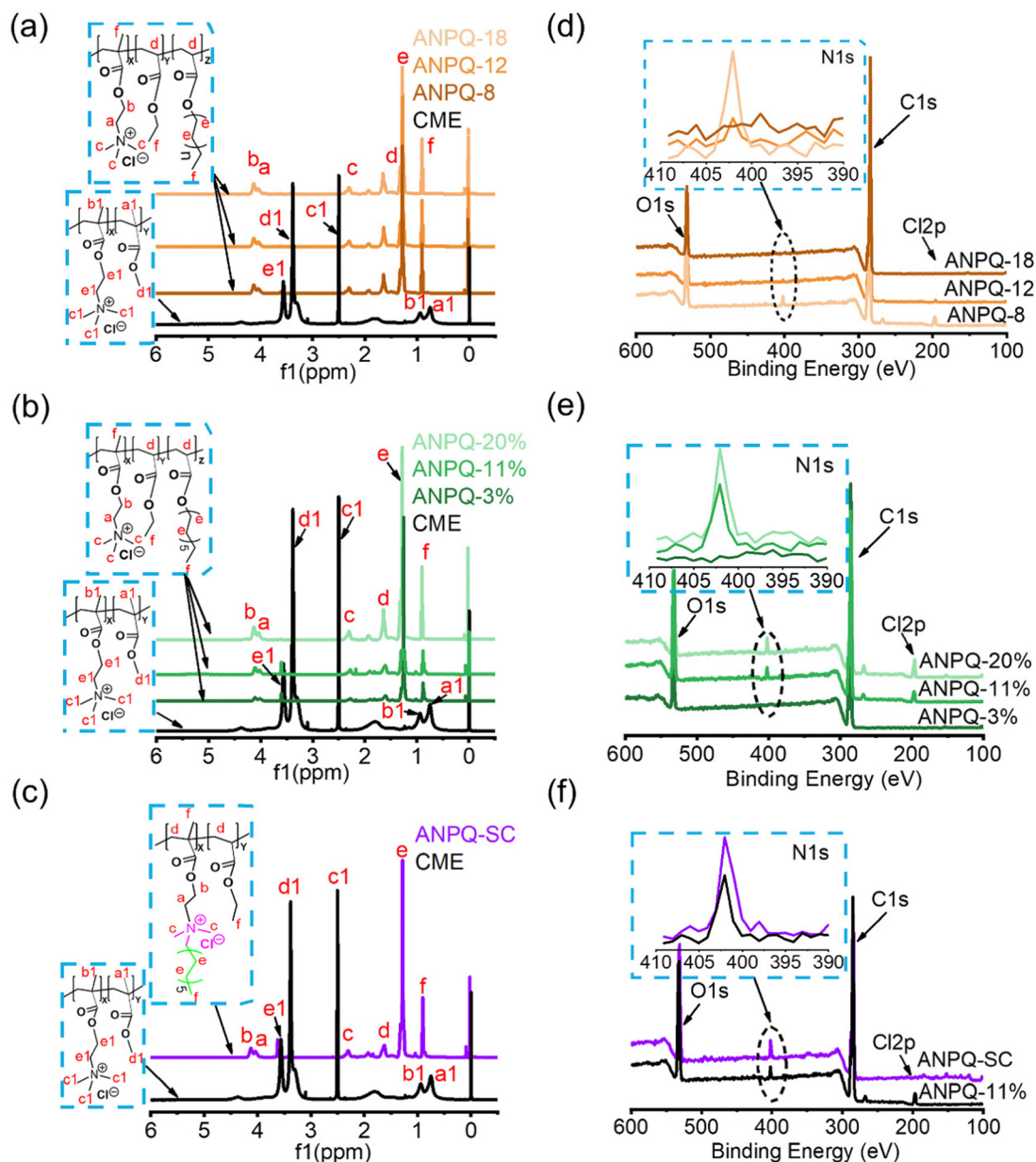
3.1 Synthesis and characterization of ANPQ

To investigate that ANPQ was synthesized as expected, the structure of ANPQ was characterized using ^{1}H NMR spectra and XPS spectra, and related data are listed in Table 2. As shown in Fig. 1a–c, the ^{1}H NMR spectra of CEM showed peaks at 3.5 ppm for $-CH_2-N^+(CH_3)_3$ and $-O-CH_2-CH_2-N^+(CH_3)_3$ groups, 3.4 ppm for $-O-CH_3$, 2.5 ppm for $-N^+(CH_3)_3$, 0.8–0.9 ppm for $-C-CH_3$ group, while in the ^{1}H NMR spectra of ANPQs at varying different alkyl chain lengths and cationic domain contents, there were peaks at 4.0–4.1 ppm for $-O-CH_2-N^+(CH_3)_3$ and $-O-CH_2-CH_2-N^+(CH_3)_3$ groups, 2.3 ppm for $-O-CH_3$ group, 1.6 ppm for $-CH_2-CH-$ group, 1.3 ppm for $-CH_2-CH_2-$ group, 0.9 ppm for $-C-CH_3$ and $-CH_2-CH_3$ groups. These results demonstrated the successful synthesis of ANPQs.

While ^{1}H NMR analysis showed the successful synthesis of ANPQs, as depicted in Scheme 1, XPS was needed to further

7754 | *J. Mater. Chem. B*, 2023, **11**, 7750–7765

This journal is © The Royal Society of Chemistry 2023

Table 2 N atomic (%), zeta potential, antibacterial activity, and biocompatibility of ANPQs

| Name | N atomic (%) | Zeta potential (mV) | MBA (mg cm^{-2}) | | | | MBA$_m$ (mg cm^{-2}) | HC50 (mg cm^{-2}) | SI |
			E. coli	S. aureus	PAO1	MRSA			
ANPQ-6	1.12	24.8 ± 1.6	>2.25	>2.25	>2.25	>2.25	2.25	9.00	3.8
ANPQ-10	0.85	26.8 ± 1.0	0.35	0.69	0.69	0.69	0.61	9.64	15.6
ANPQ-16	0.46	29.5 ± 1.7	0.32	0.64	1.28	0.64	0.73	3.06	4.2
ANPQ-3%	0.40	26.7 ± 1.9	0.98	1.95	1.95	1.95	1.71	10.36	6.0
ANPQ-11%	2.46	29.5 ± 1.1	0.35	0.69	0.35	0.69	0.52	9.76	18.8
ANPQ-20%	3.33	36.5 ± 2.7	0.27	0.13	0.54	0.27	0.30	3.26	10.8
ANPQ-SC	3.87	27.7 ± 2.3	2.35	1.18	2.35	1.18	1.77	1.18	0.6

Note: MBA$_m$ was established as the geometric mean value of MBAs; SI: Selectivity index, HA$_{50}$/MBA$_m$.

Fig. 1 Synthesis and characterization of ANPQ. (a–c) ^{1}H NMR of ANPQs. (d–f) XPS of ANPQs.

investigate the chemical structures of ANPQs. As shown in Fig. 1d–f and Table 2, the N 1s spectra of ANPQs showed that there was a peak at 401.8 eV, which was reported as the amines in their protonated states (–N$^+$(CH$_3$)$_3$).[29] With the increase in

This journal is © The Royal Society of Chemistry 2023

J. Mater. Chem. B, 2023, 11, 7750–7765 | 7755

the alkyl chain length, the intensity of N 1s spectra was decreased while it increased with the increase in the cationic domain content. As confirmed by XPS data, the N atomic content (%) of ANPQs at varying alkyl chain lengths was 1.1, 0.9, and 0.5, respectively; the N atomic content (%) of ANPQs at varying cationic domain contents was 0.4, 2.5, and 3.3, respectively. The N atomic content (%) of ANPQ-SC was 3.9.

As shown in Table 2, the values of zeta potential were 29.5 ± 1.7, 26.8 ± 1.0, 24.8 ± 1.6, 26.7 ± 1.9, 29.5 ± 1.1, 36.5 ± 2.7, and 27.7 ± 2.3 mV. With the increase in the cationic domain content, the zeta potential value increased. The high zeta potential values proved that the formation of nanoparticles increases the local density of the positive charge. The morphology of ANPQs was observed by SEM, as shown in Fig. S3 (ESI†), the nanoparticles were spherical in nature and had a size range from 250 to 500 nm after self-drying under air. These positively charged nanoparticles may easily interact with the surfaces of microbes by means of electrostatic interaction.

3.2 Antibacterial activity and antibacterial mechanism of ANPQs

The impressive antibacterial activity and biocompatibility observed in the polymers can be attributed to various factors, including the length of the side alkyl chain,[30] hydrophilic–hydrophobic balance,[31,32] as well as the linkage between functional groups.[33] By optimizing these parameters, the polymers can exhibit enhanced performance in both antibacterial activity and biocompatibility. To investigate if ANPQs and ANPQs coating posed efficient killing and good biocompatibility as predicted, the MBC and HC50 values and MBA and HA50 values were determined. As shown in Fig. S4 (ESI†) and Table 2, the antibacterial activity of ANPQs varying chain length indicated that elongation of the chain length resulted in a gradual increase in hemolysis to where hemolysis was stronger than the antimicrobial effect.[30] This was probably because the higher surface activities favor the enhancement of antibacterial activities with the increase in the alkyl chain length. However, polymers with a higher hydrophobic content are toxic to all cells and lose selectivity.[25,34,35] In Fig. S5 (ESI†) and Table 2, the MBC, MBA, HC50, and HA50 values of ANPQs decreased with the increase of cationic domain content, due to the stronger electrostatic attraction causing lower values of MBC/MBA and higher hemolysis.[31,32] ANPQ-SC with cationic groups and alkyl tails in the same center showed lower antimicrobial activity (Fig. S6, ESI†). That may be because the hydrophobic chain on the surface of ANPQ-SC plays a major role and its antimicrobial properties are limited, which was different from that described in Sen's work.[33] ANPQ-11% showed the best antibacterial activity and biocompatibility with the highest selectivity index (18.8). This was because the appropriate alkyl chain length and hydrophilic–hydrophobic balance gave excellent antimicrobial properties and biocompatibility to ANPQ-11%. Therefore, ANPQ-11% was selected for the following characterization.

To investigate why ANPQs show such great antimicrobial properties, the antibacterial mechanism was directly observed by using SEM and TEM. As shown in Fig. 2b and c, untreated PAO1 showed a complete rod-like morphology, whereas untreated MRSA exhibited a complete spherical structure. However, after incubation with ANPQ-11%, the surface of the bacteria adhered to many particles. Notably, some ANPQ-11% was partially phagocytosed and fused with the bacterial membrane structure, leaving a hemispherical indentation on the bacterial surface (Fig. 2b and c, yellow arrow). Due to the strong positive charge and the long alkyl chains, the electrostatic attraction and hydrophobic interactions between ANPQ-11% and the bacterial surface provided a favorable promotion. As a result, the strong interaction between bacterial membranes and particles caused a phagocytosis and fusion process. Since the spherical structure promoted interfacial interactions, more particles adhered.

3.3 Antibacterial activity and characterization of ANPQ coating

To confirm the utility of these polycations as antimicrobial coating materials for biomedical applications, the ANPQs were immobilized onto the PP nonwoven fabric (Fig. 3a). As shown in Fig. 3b and Fig. S7a, S8a (ESI†), ANPQ-11% nanoparticles were coated on the non-woven fabric uniformly. In ATR-FTIR spectra (Fig. 3c and Fig. S7b, S8b, ESI†), the new absorbance peak at 1727 cm^{-1} (C=O) suggested that the ANPQ-11% was successfully coated, which can be confirmed from the XPS results (Fig. 3d and e). The coating amount of ANPQ-11% was 0.47 g m^{-2} (Fig. 3f) and the surface zeta potential increased to 48.95 mV from −25.61 mV (Fig. 3g and h), which was higher than that of other ANPQs. The results indicated that the strong charge-positive property provided higher killing activity and better biocompatibility than that of other ANPQs (Fig. S7e–g and S8e–g, ESI†), which was consistent with the data from Table 2. More importantly, the water contact angle of PP$_{\text{ANPQ-11%}}$(125.08°) was nearly identical to that of pure PP (128.22°), indicating that the coating was water-insoluble.

To further investigate the superiority of the nanoparticle coating method, ANPQ-11% was coated on the wells of a 96-well plate. The coated wells treated with organic solvent were termed smooth-surface, while the coated wells without treatment were named nano-surface. As shown in Fig. 3i, the antimicrobial property of the nano-surface (MBA: 0.35 mg cm^{-2} for PAO1, 0.69 mg cm^{-2} for MRSA) was higher than that of the smooth-surface (MBA: 0.69 mg cm^{-2} for PAO1, 1.38 mg cm^{-2} for MRSA). To further study this phenomenon, SEM was conducted. After contact with the smooth surface, the cells were only slightly deformed (Fig. 3j). However, the cell structure contact with the nano-surface was significantly deformed and the cell membrane was substantially deformed and torn (Fig. 3j). This result suggested that the surface modified with nanoparticles enhanced the contact area and mechanical tension with bacteria, thus improving the antimicrobial property.[36]

3.5 Microbe adhesion and killing efficiency of ANPQ-11% coating

Medical implants and devices contaminated with MDR pathogens urgently require new coated materials. Hence, it is

7756 | *J. Mater. Chem. B*, 2023, **11**, 7750–7765

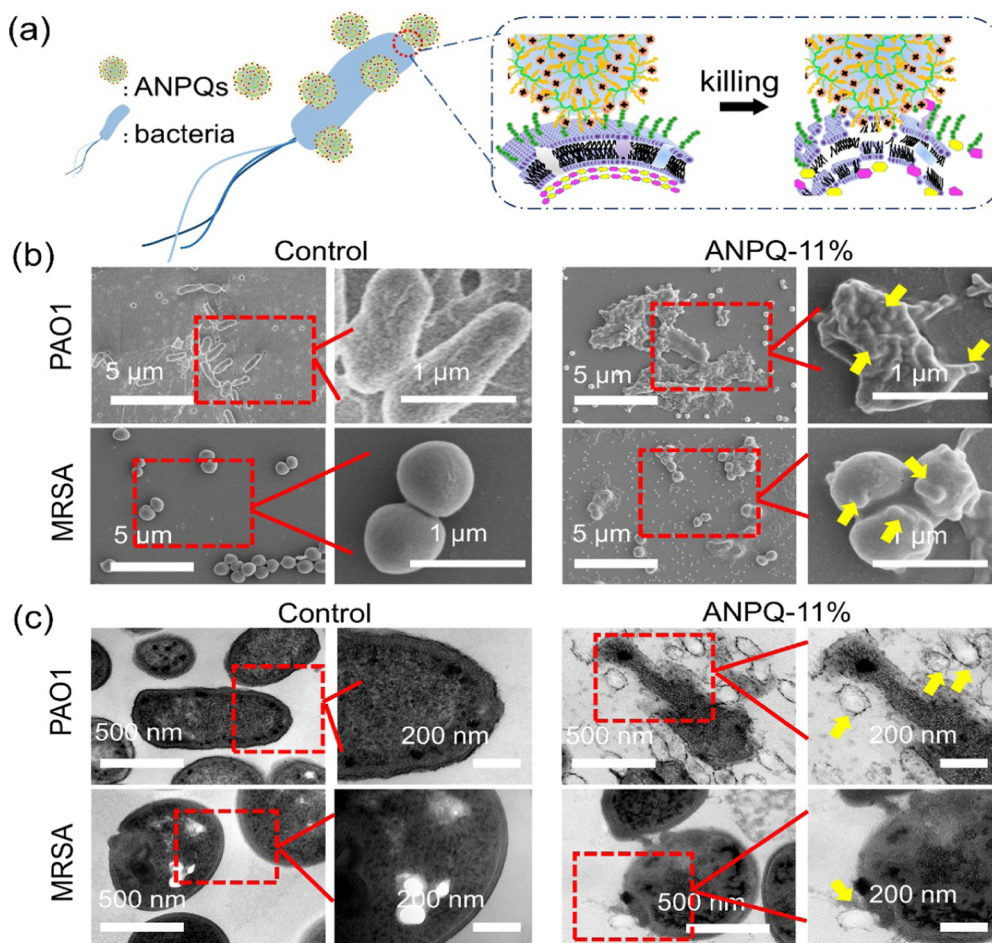This journal is © The Royal Society of Chemistry 2023

Fig. 2 (a) Scheme of ANPQs against bacteria. (b) SEM and (c) TEM of bacteria structure before and after treatment with ANPQ-11%, respectively.

necessary and critical to investigate whether the ANPQ coating exerted such an ability for enhancing the rapid adsorption-killing mechanism to combat MDR bacteria. As shown in Fig. 4a–c, untreated PP lacked the ability to absorb and kill bacteria. However, after contacting $PP_{ANPQ-11\%}$, all the bacteria in the suspension were adsorbed within 10 s. The bacterial killing ratio of $PP_{ANPQ-11\%}$ reached 99.99% after 30 s and all bacteria were killed within 1 min. ANPQ-11% coating performed noticeably better than other coating materials, such as small molecular organics,[27,37] linear quaternary ammonium salts,[11–14] inorganic nanoparticles,[38,39] metals, and metal oxide nanoparticles.[8,40–43]

To investigate the adsorption-killing mechanism of ANPQ-11% coating, the bacteria were stained with crystal violet dye under Live/Dead staining. For the $PP_{ANPQ-11\%}$ groups, the solution was completely colorless after 10 s of exposure, while the solution for PP groups was still purple even after 30 s (Fig. 4e and Movies S1, S2, ESI†). As shown in Fig. 4f, only a few bacteria adhered to PP, and the cells were still viable. However, a large number of bacteria were attached to $PP_{ANPQ-11\%}$, and the bacteria died due to the destruction of the cell membrane, which was confirmed by SEM images (Fig. S9 and S10, ESI†). Besides, after contact with PP, almost no organic matter was detected. In contrast, significant nucleic acid and protein

leakage was observed after contact with $PP_{ANPQ-11\%}$ (Fig. 4g and h). More importantly, the zone of inhibition test confirmed that ANPQ-11%-coated surfaces killed bacteria by contact rather than through leaching (Fig. S11, ESI†).

As seen in Fig. 4i, after 30 days of continuous treatment, $PP_{ANPQ-11\%}$ demonstrated a 99.99% bacterial killing rate even after only 30 seconds of contact. The surface zeta potential of $PP_{ANPQ-11\%}$ only decreased slightly from 48.95 mV to 39.33 mV (Fig. S12, ESI†). From the ATR-FTIR spectra (Fig. S13, ESI†), the absorbance at 1727 cm^{-1} (νC=O) changed little. In addition, the SEM results (Fig. S14, ESI†) further confirmed the good durability of ANPQ-11%. On the one hand, the water-insoluble property demonstrated good durability. On the other hand, ANPQ-11% interacted with PP through hydrophobic interaction, giving it long-lasting antibacterial properties. More impressively, after 2 h of contact with $PP_{ANPQ-11\%}$, the virus titer declined by 1.02 log after 2 h (Table S1, ESI†). The antiviral activity of $PP_{ANPQ-11\%}$ against the H1N1 virus highlighted its strong promise in avoiding the rapid spread of the virus in nosocomial infection.

3.6 Bacterial antimicrobial resistance of ANPQ-11% coating

Antibiotic abuse results in the spread of MDR strains associated with nosocomial infection, which has become one of the

This journal is © The Royal Society of Chemistry 2023

J. Mater. Chem. B, 2023, 11, 7750–7765 | 7757
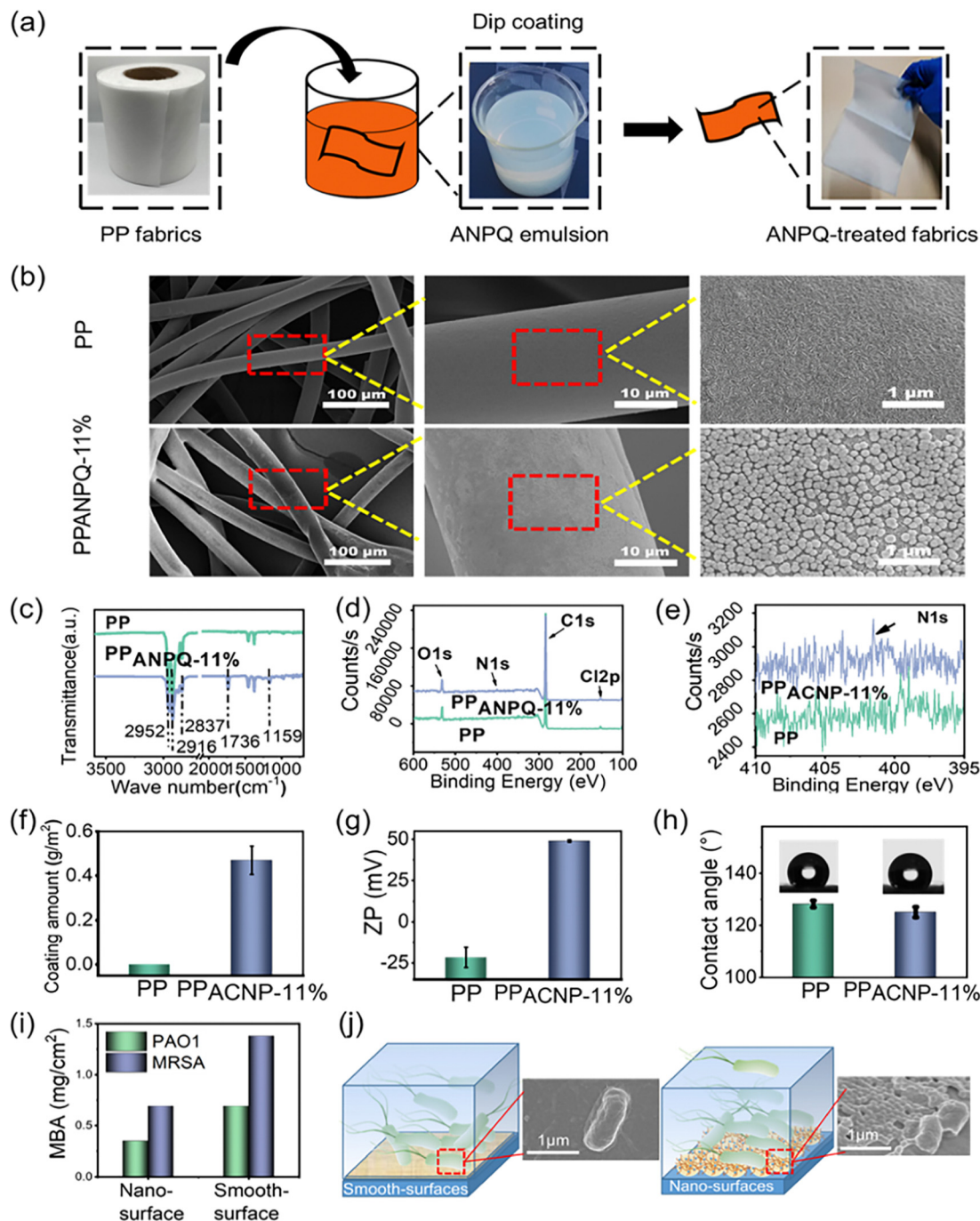
Fig. 3 Characterization of ANPQ-11% coating. (a) Coating procedure and antibacterial mechanism of PP$_{ANPQ-11\%}$. Surface properties of PP and PP$_{ANPQ-11\%}$: (c) FTIR. (d and e) XPS. (f) Coating density. (g) Surface zeta potential. (h) Contact angle. (i) MBA against PAO1 and MRSA. (j) Scheme of bacteria touched with the surface coated with ANPQ.

most severe public health threats.[44,45] Therefore, it is necessary to ensure whether incubating repeatedly with the ANPQ-11% coating results in antimicrobial resistance. As shown in Fig. 5a and b and Fig. S15 (ESI†), as compared to the antibiotic imipenem in PAO1, vancomycin in MRSA, and norfloxacin in *S. aureus*, there was no antimicrobial resistance to ANPQ-11% coating.

Surprisingly, as shown in Fig. 5c, following levofloxacin treatment, the MBA value against *E. coli* increased to 64 times that of MBA$_0$ even after 12 passages and to 256 times that of MBA$_0$ after 40 passages, suggesting significant antimicrobial resistance. In contrast, after treatment with ANPQ-11% for 40 passages, the MBA value increased slightly to 2-fold of MBA$_0$, demonstrating that the antimicrobial resistance was less likely to develop. To go deeper into the biological mechanism of bacterial response to ANPQ-11%, each group was subjected to transcriptome sequencing. As shown in Fig. 5d and e, 971 genes were differentially regulated (p value 0.05; |log 2 Fold Chang| > 0) in response to
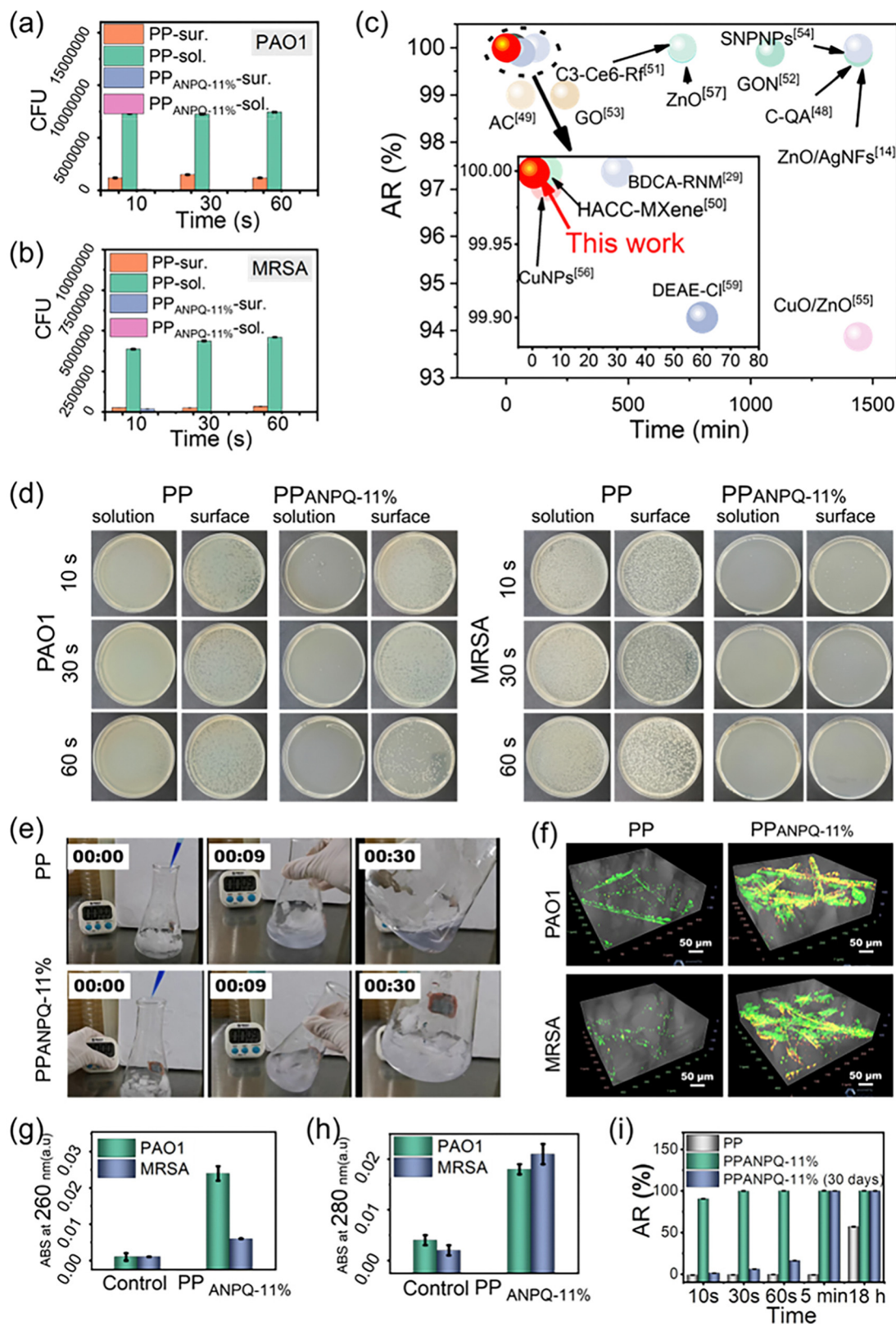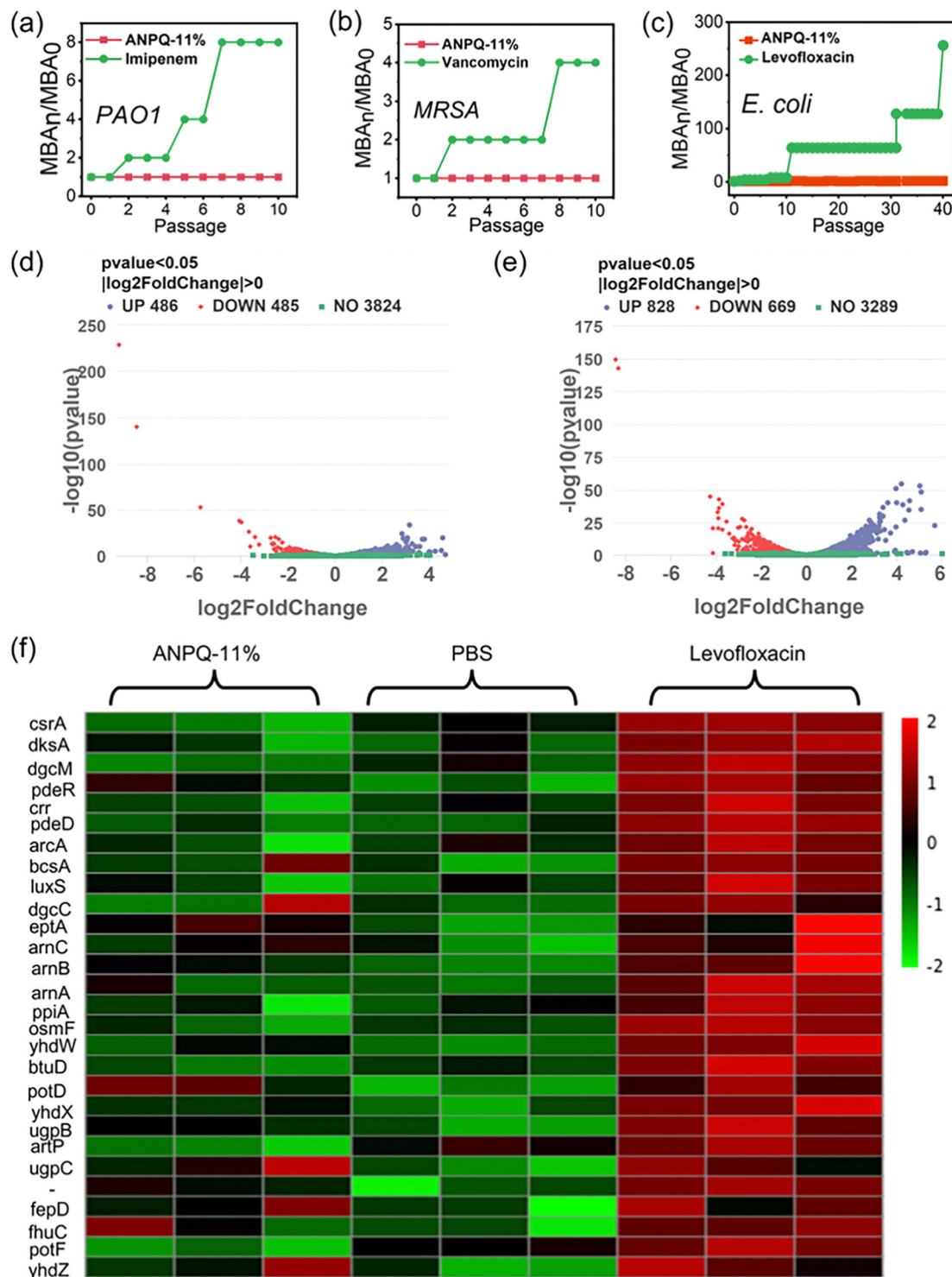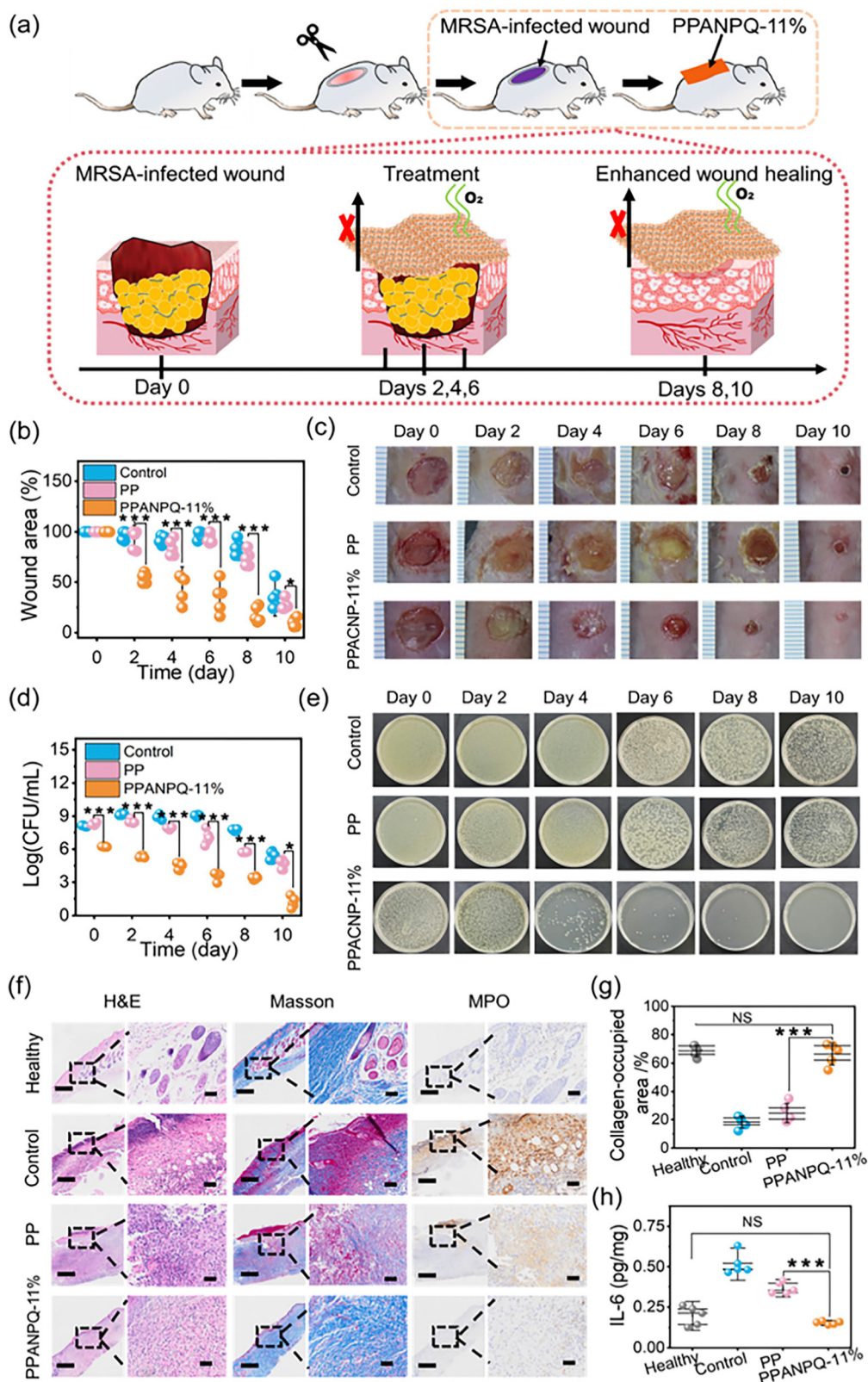
7758 | *J. Mater. Chem. B*, 2023, **11**, 7750–7765

This journal is © The Royal Society of Chemistry 2023

Fig. 4 Microbe adhesion and killing efficiency of ANPQ-11% coating. Bactericidal activity of PP$_{ANPQ-11\%}$ against (a) PAO1 and (b) MRSA. (c) Comparison of antimicrobial agent and ANPQ-11% in this work. (d) Corresponding colony images of samples. (e) Bacteria rapidly adhesion assay of PP$_{ANPQ-11\%}$. (f) CLSM images of samples. The leakage of (g) nucleic acids and (h) proteins of PAO1 and MRSA after treatment with PP$_{ANPQ-11\%}$, respectively. (i) Bactericidal activity of PP$_{ANPQ-11\%}$ against MRSA after 30 day continuous treatment.

This journal is © The Royal Society of Chemistry 2023

J. Mater. Chem. B, 2023, 11, 7750–7765 | 7759

Fig. 5 Bacterial antimicrobial resistance of ANPQ-11% coating. Development of resistance after continuous exposure to (a) PAO1 in the presence of ANPQ-11% or imipenem at 1/4-fold MBA concentration for 10 passages, (b) MRSA in the presence of ANPQ-11% or vancomycin at 1/4-fold MBA concentration for 10 passages, (c) *E. coli* 8099 in the presence of ANPQ-11% or levofloxacin at 1/4-fold MBA concentration for 40 passages. Volcano plot of differentially regulated genes following (d) ANPQ-11% and (e) levofloxacin treatment relative to untreated controls. (f) Heat cluster plots of drug resistance-related gene expression after ANPQ-11% and levofloxacin treatment were obtained by transcriptome sequencing (red: upregulated genes; green: downregulated genes).

ANPQ-11% treatment, which was significantly lower than levofloxacin (1497 genes changed). Bacterial resistance mechanisms typically include membrane-bound proteases that degrade peptides, efflux pumps, and transport systems that export cationic

7760 | *J. Mater. Chem. B*, 2023, **11**, 7750–7765

This journal is © The Royal Society of Chemistry 2023

Fig. 6 Antibacterial efficiency *in vitro*. (a) Scheme for the *in vivo* antibacterial test of PP$_{ANPQ-11\%}$ in MRSA infection mouse model; (b) quantitative measurement of the wound area in the control and PP$_{ANPQ-11\%}$ groups at different time points; (c) representative images of bacterial colonies in MRSA-infected mouse wound skin tissue; (d) bacterial colonies in (c); (e) Representative images of bacterial colonies in (c); (f) representative images of wound sections with H&E, Masson's trichrome and MPO staining on day 10 (100 µm and 50 µm); (g) collagen-occupied area by Masson staining; (h) level of IL-6 was measured by ELISA. (*$p < 0.05$, **$p < 0.01$, ***$p < 0.001$, NS: not significant.)

This journal is © The Royal Society of Chemistry 2023

*J. Mater. Chem. B*, 2023, **11**, 7750–7765 | **7761**

antimicrobial peptides (CAMPs) from periplasmic and intracellular compartments and regulation of extra-membrane permeability through outer membrane proteins, and so on.[46–48] The effect of polymers on bacterial resistance was investigated by analyzing the expression of genes closely associated with antimicrobial resistance.

According to Gene Ontology (GO) processes and Kyoto Encyclopedia of Genes and Genomes (KEGG) pathway analyses (Fig. S16–S19, ESI†), genes that are closely associated with drug resistance were selected for detailed analysis (Fig. 5f). CAMP resistance genes, such as arnB, arnC, and arnA, as well as ABC transporters (osmF, yhdW, btuD, and others), were significantly upregulated in the levofloxacin-treated groups. There were fewer distinct differentially regulated genes after treatment with ANPQ-11%, and no significant transcriptional response

was observed in any known resistance pathway (KEGG database). A series of major master regulators (including CsrA, dksA, and dgcM) of biofilm formation was significantly inhibited, indicating that the ANPQ-11% coating could inhibit adhesion and biofilm formation. Overall, antimicrobial resistance to ANPQ-11% coating was less likely to develop, which contributed to the potential for effective treatment against antimicrobial resistance.

3.7 Improved healing in an MRSA-infected wound model

Infected wound exudate contains large amounts of bacteria, which can delay wound healing and increase bacterial infection.[49] To test whether the ANPQ-treated fabrics pose such excellent adsorption-killing properties under pathological settings *in vivo*, a mouse whole-dermal MARS-infected wound
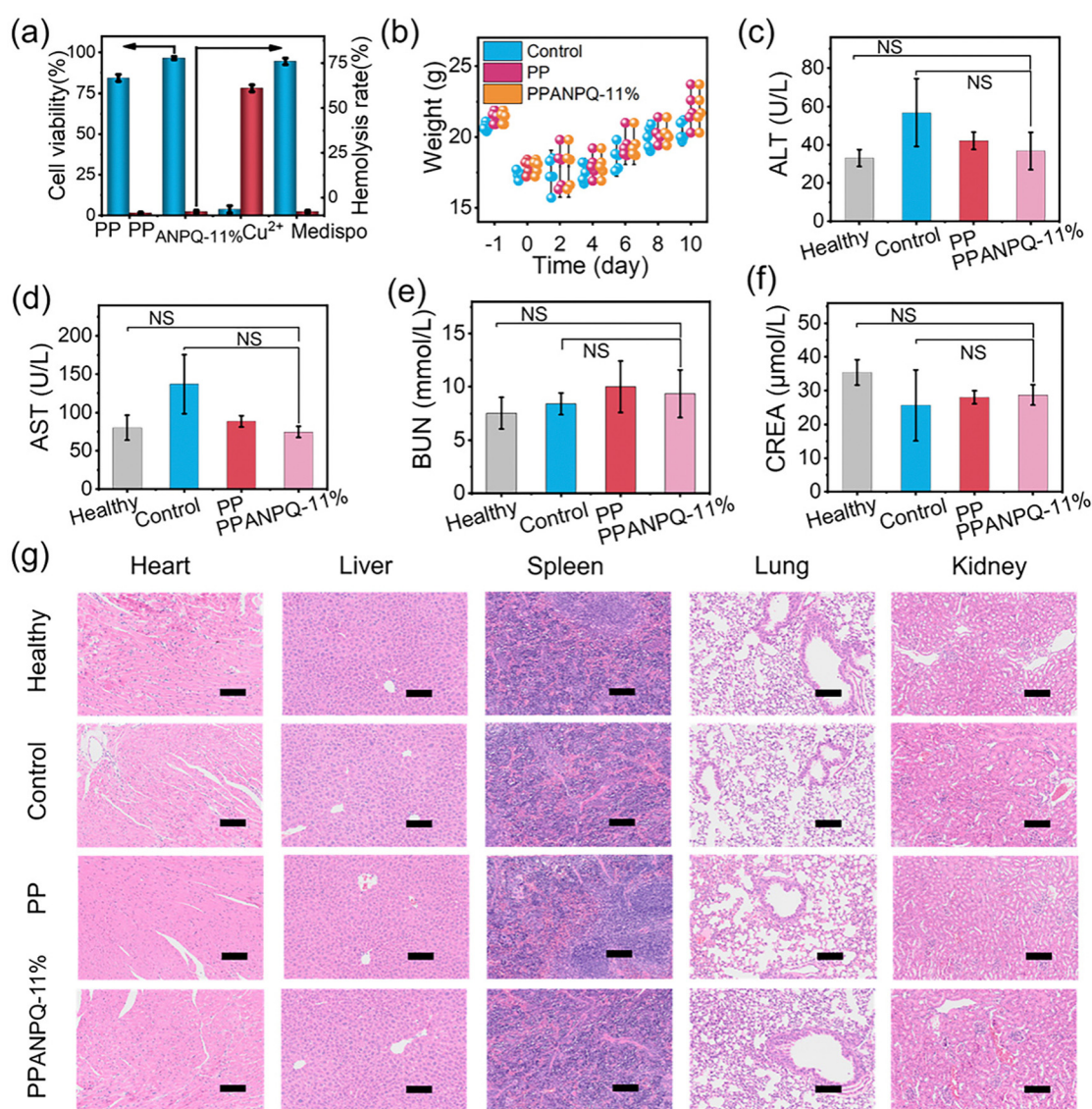
Fig. 7 Biosafety of $PP_{ANPQ-11\%}$ *in vitro* and *in vivo*. (a) Cell viability and hemolysis ratio of $PP_{ANPQ-11\%}$ and commercial nonwovens coated with copper ions or small molecule quaternary ammonium salts; (b) weight of mice in the control and PPANPQ-11% groups at different time points; (c–f) results of blood biochemistry (ALT, AST, CREA, and BUN) in different treatment groups; (g) representative images of H&E-stained tissue sections of major organs in different groups on 10th day (50 μm). (*$p < 0.05$, **$p < 0.01$, ***$p < 0.001$, NS: not significant.)

model was established(Fig. 6a). As shown in Fig. 6b–e, on the 6th day, the control groups and the PP groups continued to deteriorate and the area of the wound grew larger with swelling, pus, and blood. Additionally, the bacteria CFUs were comparable to that of the untreated wound on the first day. By contrast, on the fourth day, the PP$_{ANPQ-11\%}$ treatment group demonstrated obvious improvement. By the eighth day, the wound area was reduced to 25.6% of its initial size (**$p < 0.01$) and nearly completely healed after ten days of treatment without swelling or scabbing. Significantly, the CFUs were reduced sharply even on the second day.

To conduct in-depth research on the wound healing mechanism, wound histology sections were stained *via* H&E, Masson's trichrome, and MPO stains (Fig. 6f). Compared to the healthy groups, there was infiltration of inflammatory cells and crusting in the control groups without new granulation tissue and blood vessels growing, indicating that the wounds were more severe and difficult to heal. However, after treatment with PP$_{ANPQ-11\%}$, the wounds were almost recovered by epithelium cells, the subcutaneous tissues were reconstructed, and the inflammatory cells were reduced significantly. As shown in Fig. 6f and g, a greater amount of nascent collagen was deposited in an orientation in the PP$_{ANPQ-11\%}$ groups rather than in the control groups and the PP groups, indicating that PP$_{ANPQ-11\%}$ exerted a potent effect on accelerating wound healing.[50,51] MPO and IL-6, two powerful antibacterial proteins secreted by neutrophil granules, are linked to the body's level of inflammation, which can assess wound healing.[52,53] In Fig. 6f, MPO expression in the control groups remained high on the last day, indicating a severe wound infection. However, in the PP$_{ANPQ-11\%}$ groups, MPO tissue area was significantly reduced and expression of IL-6 (0.21 pg mg^{-1}) was obviously lower than that in the control group (0.56 pg mg^{-1}, **$p < 0.01$), suggesting that the wound tissues had entered the proliferation and remodeling stage of wound healing from the inflammatory stage (Fig. 6h). Overall, ANPQ-treated fabrics showed an excellent antimicrobial effect, and effectively promoted wound healing even in the complex environment *in vivo*.

3.8 Biosafety *in vitro* and *in vivo*.

In addition to possessing excellent antibacterial properties, the biosafety of PP$_{ANPQ-11\%}$ is also crucial. Compared with commercial nonwovens coated with copper ions or small molecule quaternary ammonium salts, PP$_{ANPQ-11\%}$ had no cytotoxicity and hemolysis (Fig. 7a and Fig. S20, ESI†). Besides, PP$_{ANPQ-11\%}$ also exhibited no skin irritation or allergy (Tables S2–S4, ESI†). During the treatment, the weight of mice in all groups increased from the 4th day (Fig. 7b). At the end of day 10, the blood collected from all groups showed that blood biochemistry results were within the normal range with no significant differences, indicating that PP$_{ANPQ-11\%}$ had no significant systemic toxicity to liver and kidney functions (Fig. 7c–g). The above *in vivo* and *in vitro* results revealed that PP$_{ANPQ-11\%}$ indicated great promise as a biocompatible antibacterial candidate to fight the spread of MDR strains associated with nosocomial infection.

4 Conclusion

In this work, we synthesized a series of amphiphilic nanoengineered polyquaternium (ANPQ) with strong electrostatic attraction and hydrophobic interactions, which showed a favorable promotion, causing bacterial phagocytosis and promoting membrane fusion. Noncovalent immobilization of the ANPQ coating provided a facile method to prevent microbial infections. Due to its water-insoluble properties, ANPQ coating demonstrated strong adhesion to the fabric with long-term durability (30 days). Surprisingly, all the bacteria were absorbed into the ANPQ-treated fabrics within only 10 s of contact, and after 30 s, the bacterial killing rate reached 99.99%. Besides, after 40 times of prolonged use, RNA-sep analysis proved that the bacteria developed resistance to levofloxacin antibiotics, but not to ANPQ-11% coating. More importantly, the ANPQ-treated fabrics exhibited excellent antibacterial properties, suggesting that the ANPQ-treated fabrics could effectively eliminate pathogens in wound exudate and facilitate skin wound healing. Moreover, nearly no cytotoxicity, hemolysis, skin irritation, and allergy were observed for ANPQ-treated fabrics, which undoubtedly made it a promising candidate for combating the spread of MDR strains.

Author contributions

Yunyun Xue, Zihao Zhao, Wenbo Huang: conceptualization, methodology, investigation, writing an original draft, data curation. Zelin Qiu, Yu Zhao, Chuyao Wang, Ronglu Cui, Shuyang Shen, Hua Tian: writing – review and editing. Xiao Li, Rong Zhou: conceptualization, methodology, resources, supervision, writing – review and editing. Lifeng Fang, Baoku Zhu: conceptualization, methodology, resources, supervision, project administration, funding acquisition.

Conflicts of interest

The authors declare that they have no known competing financial interests or personal relationships in this paper.

Acknowledgements

References

1 D. Mukwege, P. Mitangala, A. Byabene, E. Busha, Y. Van Laethem and O. Vandenberg, *Lancet*, 2022, **399**, 2348.
2 R. Laxminarayan, *Lancet*, 2022, **399**, 606–607.
3 E. Boelee, G. Geerling, B. van der Zaan, A. Blauw and A. D. Vethaak, *Acta Trop.*, 2019, **193**, 217–226.

4 *Water-Associated Infectious Diseases*, ed.S. K. Saxena, Springer Singapore, Singapore, 2020.

5 P. Singh and I. Mijakovic, *Sci. Rep.*, 2022, **12**, 7902.

6 Y. Liu, N. Peng, Y. Yao, X. Zhang, X. Peng, L. Zhao, J. Wang, L. Peng, Z. Wang, K. Mochizuki, M. Yue and S. Yang, *Nat. Commun.*, 2022, **13**, 3581.

7 Y. Jiang, W. Zheng, K. Tran, E. Kamilar, J. Bariwal, H. Ma and H. Liang, *Nat. Commun.*, 2022, **13**, 197.

8 S. Karagoz, N. B. Kiremitler, G. Sarp, S. Pekdemir, S. Salem, A. G. Goksu, M. S. Onses, I. Sozdutmaz, E. Sahmetlioglu, E. S. Ozkara, A. Ceylan and E. Yilmaz, *ACS Appl. Mater. Interfaces*, 2021, **13**, 5678–5690.

9 T. Ma, X. Zhai, Y. Huang, M. Zhang, X. Zhao, Y. Du and C. Yan, *Adv. Healthcare Mater.*, 2021, **10**, 2100033.

10 P. Westerhoff, A. Atkinson, J. Fortner, M. S. Wong, J. Zimmerman, J. Gardea-Torresdey, J. Ranville and P. Herckes, *Nat. Nanotechnol.*, 2018, **13**, 661–669.

11 L. Wang, X. Wen, X. Zhang, S. Yuan, Q. Xu, F. Fu, H. Diao and X. Liu, *Cellulose*, 2021, **28**, 5867–5879.

12 Q. Xu, L. Ying, X. Wang, Y. Zhang and P. Wang, *Fibers Polym.*, 2022, **23**, 944–953.

13 B. Yan, X. Bao, X. Liao, P. Wang, M. Zhou, Y. Yu, J. Yuan, L. Cui and Q. Wang, *ACS Appl. Mater. Interfaces*, 2022, **14**, 2132–2145.

14 L. Song, L. Sun, J. Zhao, X. Wang, J. Yin, S. Luan and W. Ming, *ACS Appl. Bio Mater.*, 2019, **2**, 2756–2765.

15 Z. Guo, S. Li, Y. Qu, J. Lu, W. Xue, X. Yu and Z. Liu, *Chem. Eng. J.*, 2021, **417**, 127970.

16 S. J. Lam, E. H. H. Wong, C. Boyer and G. G. Qiao, *Prog. Polym. Sci.*, 2018, **76**, 40–64.

17 L.-Z. Su, Y. Liu, Y.-F. Li, Y.-L. An and L.-Q. Shi, *Chin. J. Polym. Sci.*, 2021, **39**, 1376–1391.

18 T. Selkälä, T. Suopajärvi, J. A. Sirviö, T. Luukkonen, P. Kinnunen, K. I. Kling, J. B. Wagner and H. Liimatainen, *Chem. Eng. J.*, 2019, **374**, 1013–1024.

19 F. Nederberg, Y. Zhang, J. P. K. Tan, K. Xu, H. Wang, C. Yang, S. Gao, X. D. Guo, K. Fukushima, L. Li, J. L. Hedrick and Y.-Y. Yang, *Nat. Chem.*, 2011, **3**, 409–414.

20 J. M. V. Makabenta, A. Nabawy, C.-H. Li, S. Schmidt-Malan, R. Patel and V. M. Rotello, *Nat. Rev. Microbiol.*, 2021, **19**, 23–36.

21 S. J. Lam, N. M. O'Brien-Simpson, N. Pantarat, A. Sulistio, E. H. H. Wong, Y.-Y. Chen, J. C. Lenzo, J. A. Holden, A. Blencowe, E. C. Reynolds and G. G. Qiao, *Nat. Microbiol.*, 2016, **1**, 16162.

22 S. Tian, H. C. van der Mei, Y. Ren, H. J. Busscher and L. Shi, *J. Mater. Sci. Technol.*, 2021, **84**, 208–218.

23 Y. K. Jo, J. H. Seo, B.-H. Choi, B. J. Kim, H. H. Shin, B. H. Hwang and H. J. Cha, *ACS Appl. Mater. Interfaces*, 2014, **6**, 20242–20253.

24 F. Wu, G. Meng, J. He, Y. Wu, F. Wu and Z. Gu, *ACS Appl. Mater. Interfaces*, 2014, **6**, 10005–10013.

25 J. Hoque, P. Akkapeddi, V. Yadav, G. B. Manjunath, D. S. S. M. Uppu, M. M. Konai, V. Yarlagadda, K. Sanyal and J. Haldar, *ACS Appl. Mater. Interfaces*, 2015, **7**, 1804–1815.

26 J. Lin, X. Chen, C. Chen, J. Hu, C. Zhou, X. Cai, W. Wang, C. Zheng, P. Zhang, J. Cheng, Z. Guo and H. Liu, *ACS Appl. Mater. Interfaces*, 2018, **10**, 6124–6136.

27 Y. Si, Z. Zhang, W. Wu, Q. Fu, K. Huang, N. Nitin, B. Ding and G. Sun, *Sci. Adv.*, 2018, **4**, eaar5931.

28 C. Z. Chen and S. L. Cooper, *Biomaterials*, 2002, **23**, 3359–3368.

29 J. Ederer, P. Janoš, P. Ecorchard, J. Tolasz, V. Štengl, H. Beneš, M. Perchacz and O. Pop-Georgievski, *RSC Adv.*, 2017, **7**, 12464–12473.

30 T. N. Siriwardena, M. Stach, R. He, B.-H. Gan, S. Javor, M. Heitz, L. Ma, X. Cai, P. Chen, D. Wei, H. Li, J. Ma, T. Köhler, C. van Delden, T. Darbre and J.-L. Reymond, *J. Am. Chem. Soc.*, 2018, **140**, 423–432.

31 S. Zhao, W. Huang, C. Wang, Y. Wang, Y. Zhang, Z. Ye, J. Zhang, L. Deng and A. Dong, *Biomacromolecules*, 2020, **21**, 5269–5281.

32 E. F. Palermo, K. Lienkamp, E. R. Gillies and P. J. Ragogna, *Angew. Chem., Int. Ed.*, 2019, **58**, 3690–3693.

33 V. Sambhy, B. R. Peterson and A. Sen, *Angew. Chem., Int. Ed.*, 2008, **47**, 1250–1254.

34 S. Colak, C. F. Nelson, K. Nüsslein and G. N. Tew, *Biomacromolecules*, 2009, **10**, 353–359.

35 E. F. Palermo, I. Sovadinova and K. Kuroda, *Biomacromolecules*, 2009, **10**, 3098–3107.

36 C. Q. Lai, *Langmuir*, 2018, **34**, 4059–4070.

37 P. Tang, Z. Zhang, A. Y. El-Moghazy, N. Wisuthiphaet, N. Nitin and G. Sun, *ACS Appl. Mater. Interfaces*, 2020, **12**, 49442–49451.

38 F. Yaghoubidoust and E. Salimi, *Fibers Polym.*, 2019, **20**, 1155–1160.

39 J. Zhao, B. Deng, M. Lv, J. Li, Y. Zhang, H. Jiang, C. Peng, J. Li, J. Shi, Q. Huang and C. Fan, *Adv. Healthcare Mater.*, 2013, **2**, 1259–1266.

40 B. R. Rao, R. Kumar, S. Haque, J. M. Kumar, T. N. Rao, R. V. S. N. Kothapalli and C. R. Patra, *ACS Appl. Mater. Interfaces*, 2021, **13**, 10689–10704.

41 G. Guan, L. Zhang, J. Zhu, H. Wu, W. Li and Q. Sun, *J. Hazard. Mater.*, 2021, **402**, 123542.

42 S. Kumar, M. Karmacharya, S. R. Joshi, O. Gulenko, J. Park, G.-H. Kim and Y.-K. Cho, *Nano Lett.*, 2021, **21**, 337–343.

43 X. Ni, C. Li, Y. Lei, Y. Shao, Y. Zhu and B. You, *ACS Appl. Mater. Interfaces*, 2021, **13**, 57864–57879.

44 The EuSCAPE Working Group, the ESGEM Study Group, S. David, S. Reuter, S. R. Harris, C. Glasner, T. Feltwell, S. Argimon, K. Abudahab, R. Goater, T. Giani, G. Errico, M. Aspbury, S. Sjunnebo, E. J. Feil, G. M. Rossolini, D. M. Aanensen and H. Grundmann, *Nat. Microbiol.*, 2019, **4**, 1919–1929.

45 O. O. Ikhimiukor, E. E. Odih, P. Donado-Godoy and I. N. Okeke, *Nat. Microbiol.*, 2022, **7**, 757–765.

46 Y. Gao, J. Wang, M. Chai, X. Li, Y. Deng, Q. Jin and J. Ji, *ACS Nano*, 2020, **14**, 5686–5699.

47 Y. Yu, J. Dong, Y. Wang and X. Gong, *PeerJ*, 2021, **9**, e11081.

48 W. Chin, G. Zhong, Q. Pu, C. Yang, W. Lou, P. F. De Sessions, B. Periaswamy, A. Lee, Z. C. Liang, X. Ding, S. Gao, C. W. Chu, S. Bianco, C. Bao, Y. W. Tong, W. Fan, M. Wu, J. L. Hedrick and Y. Y. Yang, *Nat. Commun.*, 2018, 9, 917.

49 B. A. Mast and G. S. Schultz, *Wound Repair Regener.*, 1996, **4**, 411–420.

50 J. Wu, J. Zhu, C. He, Z. Xiao, J. Ye, Y. Li, A. Chen, H. Zhang, X. Li, L. Lin, Y. Zhao, J. Zheng and J. Xiao, *ACS Appl. Mater. Interfaces*, 2016, **8**, 18710–18721.

51 W. Gao, W. Jin, Y. Li, L. Wan, C. Wang, C. Lin, X. Chen, B. Lei and C. Mao, *J. Mater. Chem. B*, 2017, **5**, 7285–7296.

52 S. Kongkiatkamon, L. Terkawi, Y. Guan, V. Adema, M. Hasipek, T. Dombrovski, M. Co, W. Walter, H. Awada, Y. Parker, S. Hutter, S. Pagliuca, C. Gurnari, H. J. Rogers, M. Meggendorfer, D. J. Lindner, T. Haferlach, V. Visconte, T. LaFramboise, B. K. Jha and J. P. Maciejewski, *Leukemia*, 2022, **36**, 2086–2096.

53 T. M. Kistner, B. K. Pedersen and D. E. Lieberman, *Nat. Metab.*, 2022, **4**, 170–179.

This journal is © The Royal Society of Chemistry 2023

J. Mater. Chem. B, 2023, **11**, 7750–7765 | **7765**